Biomimetic Synthesis

DOI: 10.1002/ange.200900437

From Metal Binding to Nanoparticle Formation: Monitoring Biomimetic Iron Oxide Synthesis within Protein Cages using Mass Spectrometry**

Sebyung Kang, Craig C. Jolley, Lars O. Liepold, Mark Young, and Trevor Douglas**

Biomimetic nanomaterials syntheses utilizing protein cages, including ferritins, viruses, and heat shock proteins, have been widely used to provide a high degree of control over the particle morphology, composition, and polymorph selection under relatively mild synthetic conditions.[1–5] However, the processes of metal ion accumulation and nanoparticle formation coupled to the protein cage are still poorly understood.

In this study we have investigated the process of biomimetic iron oxide nanoparticles synthesis within protein cages using noncovalent mass spectrometry (NCMS). Accurate mass measurements of metal-mineralized protein cages allowed us, for the first time, to quantitatively examine the effects of metal ion concentration on the final nanoparticle size. Imaging of iron oxide nanoparticles using transmission electron microscopy (TEM) provides further information about nanoparticle sizes, confirming the NCMS results. A kinetic master equation-based model was used to infer the molecular details of metal ion accumulation and nanoparticle formation from these final reaction products. Modeling results suggest that particle growth involves both a binding phase (with growth rate limited by ion accumulation) and a growth phase (with growth rate proportional to the particle surface area).

Unlike most other analytical techniques, mass spectrometry can simultaneously detect different molecular masses present in a mixture. Thus, mass spectrometry can detect multiple transient populations and monitor their changes individually. The combination of electrospray ionization (ESI) and time-of-flight (TOF) mass analyzer makes it possible to measure the mass of intact noncovalently associated macromolecular complexes without disturbing structures as well as the masses of individual protein components.[6–10] We have used this approach to monitor the process of metal ion accumulation and iron oxide nanoparticles formation within a protein cage at the molecular level.

The LiDps (*D*NA binding *p*rotein from *s*tarved cells from the Gram-negative bacterium *Listeria innocua*) is a member of the ferritin superfamily and composed of 12 identical 18 kDa subunits with an outer diameter of 9 nm and an inner cavity diameter of 5 nm (Figure 1).[11] LiDps produces an iron oxide core, similar to that of typical ferritins, to protect cellular DNA from oxidative stress.[11–13] Using biomimetic approaches, LiDps has been used as a template for the synthesis of nanomaterials of iron[14] and cobalt oxide[15] as well as cadmium sulfide[16] and platinum.[17]

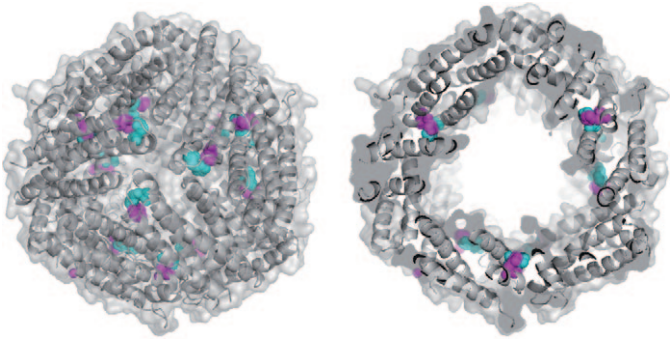

Figure 1. Surface and ribbon-diagram representations of LiDps (PDB 1QGH) looking down the three-fold symmetry axis (left) and a clipped view showing the interior space of the cage (right). Histidine 31 (magenta) and 43 (cyan) residues are represented as spheres.

Fe^{II} binding to LiDps has been extensively studied by spectroscopic methods under anaerobic conditions.[12,13,18] It has been proposed that LiDps has metal-binding centers located at the two-fold symmetric subunit interfaces and demonstrated that mutations of both metal-binding centers (H31, H43) diminished Fe^{II} binding to LiDps under anaerobic conditions.[13]

Although LiDps biomineralizes Fe as a nanoparticle of amorphous ferric oxyhydroxide under physiological conditions, treatment of LiDps at pH 8.5 and 65 °C with 400 Fe^{II} per cage and substoichiometric amounts of H_2O_2 (2:1, $Fe:H_2O_2$) resulted in the formation of maghemite (γ-Fe_2O_3) as identified by electron powder diffraction.[14] This biomimetic synthesis allows the formation of well-defined crystalline nanoparticles with narrow size distributions within LiDps. Now we have utilized this chemistry in conjunction with NCMS to

[*] Prof. M. Young
Department of Plant Science, Montana State University
Fax: (+1) 406-994-5117
E-mail: myoung@montana.edu
Dr. S. Kang, Dr. C. C. Jolley, L. O. Liepold, Prof. T. Douglas
Department of Chemistry and Biochemistry
Center for BioInspired Nanomaterials
Montana State University, Bozeman, MT 59717 (USA)
Fax: (+1) 406-994-5947
E-mail: tdouglas@chemistry.montana.edu

[**] This research was supported in part by grants from HFSP (RGP61/2007), the NSF (CBET-0709358), ONR (N00014-03-1-0692), and DOE (DE-FG02-07ER46477).

Supporting information for this article is available on the WWW under http://dx.doi.org/10.1002/anie.200900437.

follow the processes of biomimetic Fe mineralization within the LiDps protein cage.

Various amounts of Fe^{II} (24, 48, 100, 200, and 400 Fe^{II} per cage) were added together with a half equivalent of H_2O_2 slowly over 15 min. The reaction chambers were maintained at pH 8.5 and 65 °C using a pH titrator and a heated water jacket. Each of the reaction products was analyzed by size-exclusion chromatography (SEC). Elution profiles confirmed co-elution of protein cages and iron oxide nanoparticles regardless of the initial loading amounts of Fe^{II} ions (Figure 1 in the Supporting Information). UV/Vis spectra of selected protein cage fractions clearly showed an increase in absorbance with increasing initial Fe^{II} loading (Figure 1 in the Supporting Information) suggesting that sufficiently large iron oxides are formed with high Fe^{II} loading. Electron micrographs of negatively stained Fe-mineralized LiDps revealed an intact cagelike structure, with an outer diameter of (9 ± 0.5) nm $l = (5.3478 \pm 0.0065)$ cm (Figure 2 A). Distinct

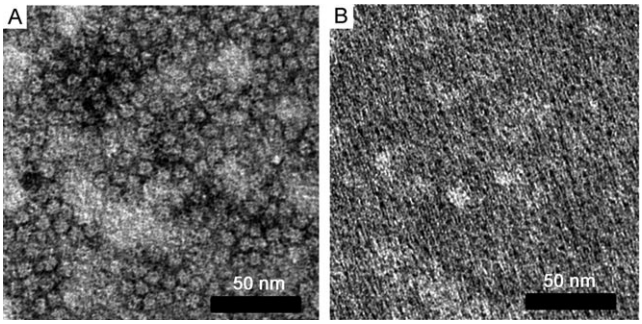

Figure 2. Transmission electron micrographs of 400 Fe^{II} loaded LiDps stained with 2% uranyl acetate (A) and unstained (B).

particles of iron oxide [(2.7 ± 0.4) nm diameter] were observed with loading factors of 400 Fe^{II} per LiDps without staining (Figure 2 B). While dense cores were also frequently detected with 200 Fe^{II} loaded LiDps, we could not accurately determine the particle size, because it was close to the marginal resolution limit of our TEM (< 2 nm). No distinctive electron-dense cores were detected in samples with 100 or less Fe^{II} loadings (data not shown).

To determine the absolute number of bound Fe ions or the size of iron oxides within the LiDps at varying initial Fe loadings, we performed NCMS analyses with the Fe-mineralized LiDps. SEC-separated Fe-mineralized LiDps were subjected to mass spectrometric analyses. ESI generally produces a series of multiply charged ions and the charges (z) are generally distributed as a continuous series with a Gaussian intensity distribution (…, $z-2$, $z-1$, z, $z+1$, $z+2$, …; Figure 3 A, bottom panel). If there are multiple species in a mass spectrum, multiple Gaussian charge distributions can be detected and the molecular masses of each species can be determined from the charges and the observed mass-to-charge (m/z) ratios (see the Supporting information for details). Charge-state distributions of Fe-mineralized LiDps shifted to higher m/z values according to the increase of initial Fe^{II} loadings (Figure 3 A). While each peak was well resolved with Fe^{II} loadings of 100 or less, all peaks were merged into a broad peak for higher loadings. These samples with 200 and 400 Fe^{II} loadings (where iron oxide nanoparticles were seen under TEM) show indistinct mass spectra probably due to broadening of each peak caused by the heterogeneity in the iron oxide particle sizes beyond the resolution of mass spectrometry (Figure 3 A). For the smaller particles where peak resolution was possible, the peak shapes suggest the presence of more than one mass distribution for each charge state (Figure 3 A, B).

To follow the individual species within the ensemble population, mass spectra were fit with either one (untreated cages) or two Gaussian functions (Fe^{II} treated cages) because two major species clearly were resolved with 100 Fe^{II} loaded LiDps. All charge-state peaks exhibited the same peak broadening and splitting (Figure 3 A) and we selected the most intense peak (22 +) for data fitting (Figure 3 B). With 24 Fe^{II} loading, where no absorption at 350 nm was observed (Figure 1 in the Supporting Information), the 22 + charge-state peak was decomposed as two major peaks, m/z 9872 and 9888, which correspond to mass increases of 330 and 682 Da, respectively (Figure 3 B). Similar to 24 Fe^{II} loading, peaks were decomposed as two major peaks for 48 and 100 Fe^{II} loadings, m/z 9888 and 9922 and m/z 9886 and 10000, which correspond to mass increases of 682 and 1430 Da and 638 and 3146 Da, respectively (Figure 3 B).

The numbers of Fe ions and Fe_2O_3 molecules, converted from the observed individual mass increases, are listed in Table 1. Although each peak shows a different splitting pattern, one common peak was observed at m/z 9888 corresponding to approximately 12 Fe ions in all samples. Interestingly, this number matches with the previously reported number of Fe ions bound.[12,13,18] This common charge-state cluster was also detected in the mass spectra of 200 and 400 Fe^{II} loaded LiDps (Figure 3 A, arrows on the top and second top panels). These results suggest that a population of LiDps containing 12 Fe ions, bound at the ferroxidase centers, is formed at very early mineralization stages. In addition, this long-lived Fe accumulating intermediate state may be a prerequisite stage for further iron oxide nanoparticle formation. A ferroxidase center knock-out mutant did not mineralize iron oxide under the same condition (Figure 2 in the Supporting Information), strongly supporting that this early 12 Fe accumulating stage is indeed necessary for successful maghemite nanoparticle formation within the protein cage.

In the case of 200 and 400 Fe^{II} loadings, charge-state distributions clearly shifted to higher m/z values to different degrees. However, it was not possible to determine accurate masses from the NCMS data alone, because they did not have well-resolved charge-state peaks as were seen with lower initial Fe^{II} loadings. For these larger particles, however, it was possible to measure maghemite nanoparticle sizes using TEM and to calculate particle masses based on the known density of crystalline maghemite.[19] The unit cell volume of maghemite is 0.58 nm^3 and the cell contains 21 Fe atoms.[19] By TEM we observed maghemite within LiDps with diameters of (2.7 ± 0.4) nm. This translates to a mineral volume of approximately 10.3 nm^3 and 186 Fe_2O_3 (372 Fe atoms with a loading of 400 Fe^{II} per cage). We also observed a small degree

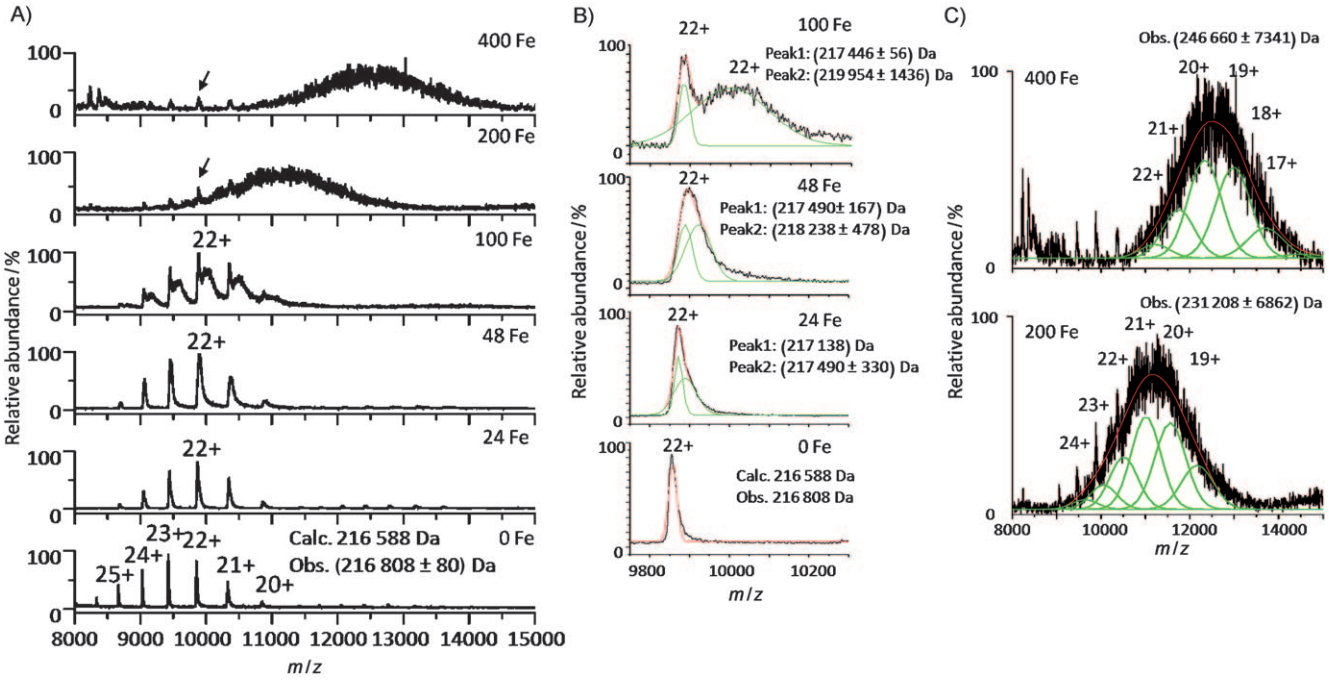

Figure 3. A) Mass spectra of Fe-mineralized wild-type (wt) LiDps at various loading ratios of Fe^{II}. Charged peaks are indicated in the bottom spectrum. B) Fittings (red) of 22+ peaks of Fe-mineralized wt LiDps at lower loads either with one (0 Fe^{II}) or two Gaussians (green). C) Fittings (red) of mass spectra of Fe-mineralized wt LiDps at 200 and 400 Fe^{II} per cage with six Gaussians (green). Charge-state peaks and calculated masses are indicated.

Table 1: Numbers of Fe ions and Fe_2O_3 converted from the observed mass increases at various initial Fe^{II} loads.[a]

Load per cage	Fe ions		Fe_2O_3
	Peak 1	Peak 2	
24 Fe	5.9 (37%)	12.2 ± 6 (63%)	
48 Fe		12.2 ± 3 (35%)	8.9 ± 3 (65%)
100 Fe		11.4 ± 1 (13%)	19.7 ± 9 (65%)
200 Fe		12 (< 1%)	90 ± 43
400 Fe		12 (< 1%)	186 ± 46

[a] Relative amounts (in %) were calculated by integrating peak areas, and deviations were determined by calculating the half-width at the half-height of each peak.

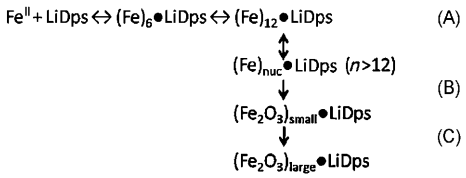

Scheme 1. A proposed mechanism for the process of biomimetic iron oxide synthesis within LiDps cages.

of charge-state shift upon Fe^{II} treatments (the most intense peak shifts from 23+ to 22+ upon iron treatments, Figure 3A, bottom panel to second bottom). It is reasonable to assume that only one or two charge shifts occur upon formation of large iron oxide nanoparticles within LiDps. Therefore, the whole mass spectra of 200 and 400 Fe^{II} loaded LiDps were fit with six broad peaks with the most intense peaks at charge 21+ (m/z 11011) and 20+ (m/z 12334) which correspond to mass increases of 14400 and 29852 Da and translate to 90 Fe_2O_3 (180 Fe ions) and 186 Fe_2O_3 (372 Fe ions), respectively (Figure 3C, Table 1).

Taking all the data together, we propose a mechanism for the biomimetic iron oxide synthesis within LiDps. At low Fe^{II} loadings, the ions are introduced and distributed evenly into LiDps such that up to 12 Fe ions (either Fe^{II} or Fe^{III}) accumulate in each cage through the whole population of apo-LiDps (Scheme 1A). A subpopulation of the cages obtains a limited amount of Fe (6 Fe with 24 Fe^{II} loadings, Figure 3B and Table 1) presumably due to depletion of available Fe^{II} ions (Scheme 1A). With intermediate Fe^{II} loading, the binding sites are completely occupied and those cages accumulating Fe beyond some critical amount (short-lived nucleating intermediate, $(Fe)_{nuc}$•LiDps) begin to form small iron oxide nanoparticles (Scheme 1B). However, the short-lived nucleating intermediate was not detected in the final reaction products we examined presumably due to its rapid transition to an iron oxide particle. Sufficiently large amounts of Fe^{II} loading allows full occupation of the binding sites followed by initiation of small iron oxide formation. Subsequently, the surface of small iron oxides may dominate iron oxide growth, through autocatalysis, resulting in the formation of larger iron oxide nanoparticles (Scheme 1C). A small subpopulation of the cages may not reach the critical Fe accumulation point ($(Fe)_{nuc}$•LiDps) and will remain with only 12 Fe ions bound (long-lived intermediate; Scheme 1).

We have developed a simple kinetic model for this two-stage growth process to make this Scheme more quantitative. While our experimental data do not include direct measure-

ment of kinetics, it is clear from modeling efforts that the observable reaction products are determined by kinetic parameters. Let $[np_i]$ represent the concentration of iron oxide nanoparticles containing i Fe atoms; the array of $[np_i]$ forms a histogram of particle sizes. The process of growth occurring during an interval Δt can be written as Equations (1) where [Fe] is the instantaneous iron concentration in

$$\Delta[np_i] = [Fe]\Delta t(k_i[np_{i-1}] - k_{i+1}[np_i])$$
$$\Delta[Fe] = -[Fe]\Delta t \sum_i k_i[np_i] \quad (1)$$

bulk and k_i is the rate constant for particles with i Fe atoms. The first equation in (1) indicates that $[np_i]$ increases as $[np_{i-1}]$ is depopulated and decreases as $[np_{i+1}]$ becomes populated. The second indicates that particle growth always leads to decreases in [Fe]. Thus far, the model assumes that growth proceeds one atom at a time (for small enough values of Δt) and that iron incorporation is irreversible. We approximate k_i according to Equation (2).

$$k_i = \begin{cases} k_{binding} & \text{if} \quad i \le N_{acc} \\ k_{growth}A_i & \text{if} \quad N_{acc} < i < N_{max} \\ 0 & \text{if} \quad i \ge N_{max} \end{cases} \quad (2)$$

In the first case, where $i \le N_{acc}$, Fe accumulation is diffusion-limited and k_i is constant ($k_{binding}$). Based on our NCMS results and previous reports,[12,13,18] we set $N_{acc} = 12$, the number of ions that can bind prior to particle formation. Once a maghemite nanoparticle begins to form within the cage, further growth is catalyzed by the surface of the particle (k_{growth}). The growth rate is proportional to the particle surface area A_i; if we assume spherical particles, we can further approximate $A_i \propto i^{2/3}$. Finally, if the particle size reaches N_{max}, the growth of the maximum number of Fe atoms that can be contained in the cage stops. In practice, particle sizes near N_{max} are inaccessible due to protein instability at very high [Fe] and size truncation effects are not observed. Since only the final reaction products are examined, the model effectively only contains one free parameter; the ratio between $k_{binding}$ and k_{growth}. Various ratios (1.1:1–60:1) were modeled and the resulting distribution widths and positions were compared to data collected from NCMS (Figure 3 in the Supporting Information). The value of $k_{binding}/k_{growth}$ was optimized to 2.91:1, giving an $R^2 = 0.88$ fit to the experimental data (Figure 4 in the Supporting Information), and used for generating a time series of particle size (number of Fe atoms) histograms (Figure 4). The particle-size distributions were found numerically by starting with nonzero values of [Fe] and $[np_0]$ (with $[np_i] = 0$ for $i > 0$) and updating [Fe] and the $[np_i]$ array iteratively until a steady state was reached. Under experimentally relevant conditions, the reaction continued until [Fe] = 0 and a histogram of $[np_i]$ showed a bimodal distribution reminiscent of the experimental NCMS data (Figure 4 and inset).

In summary, we have been able to demonstrate detection of biomimetic Fe oxide nanoparticles at a range of sizes, depending on the Fe loading ratio. To our knowledge, this is the first report to determine the sizes of biomimetically

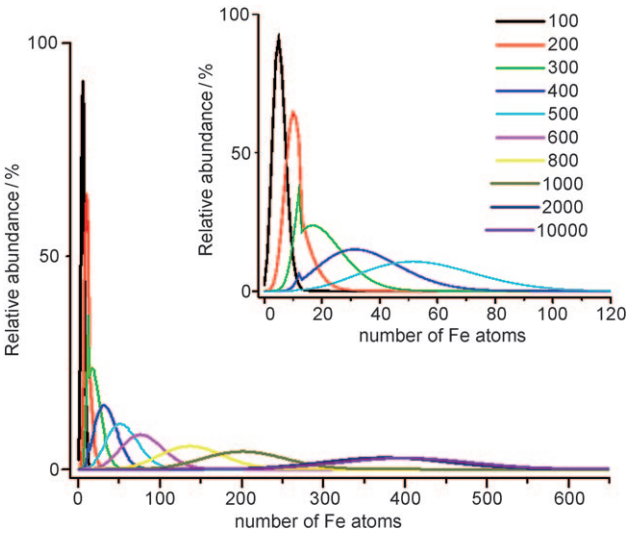

Figure 4. Time series of particle growth for a loading ratio of 400 Fe atoms per cage. Inset: Increased detail for the early-time region. The bimodal distribution is especially clear for the histograms at 300 and 400 steps.

synthesized nanoparticles at molecular size ranges, from metal accumulation to visible metal oxide nanoparticles. By combining experimental and modeling efforts, we can gain information about early stages of Fe binding and its subsequent conversion into iron oxide nanoparticles. These results allow us to build a quantitative model of this transformation that can easily be applied to other mineralization reactions.

Experimental Section

Mutagenesis and protein purification: Histidines at residues 31 and 43 were replaced by glycines (H31G,H43G) using sequential polymerase chain reaction protocols to generate knock-out mutants as previously described.[13] The double knock-out mutant (H31G,H43G) and wt LiDps protein cages were over-expressed in *E. coli* and purified as described previously.[14]

Maghemite synthesis:[14] 1 mg of the LiDps protein cages was added to a de-aerated solution of 0.1 M NaCl (2 mL final) in a jacketed reaction vessel under N_2. The temperature was maintained at 65 °C by circulating water through the jacketed flask. The reaction was brought to pH 8.5 using a de-aerated solution of 0.1 M NaOH (Brinkman 718 AutoTitrator). 300 μL of the appropriate concentrations of de-aerated solutions of iron ($(NH_4)_2Fe(SO_4)_2{\cdot}H_2O$) and oxidant ($H_2O_2$, half the concentration of iron solution) were added simultaneously at a rate of 20 μL min^{-1} to achieve the theoretical loadings of 24, 48, 100, 200, or 400 Fe^{II} per cage using a syringe pump (Kd Scientific). Iron and oxidant solutions were added over 15 min and the reactions were maintained for 5 more minutes to complete reactions. Reactions were loaded onto a 10 × 300 mm Superose 6 (Amersham Bioscience) size-exclusion column and eluted with buffer containing 50 mM 4-morpholineethanesufonic acid (MES), 100 mM NaCl (pH 6.5) at a rate of 0.5 mL min^{-1}.

Mass spectrometry: Mass analyses of the intact and metal-treated LiDps were carried out on samples in 10 mM TEAA, pH 6.8 under the same mass spectrometry condition as described previously.[17,20] Charge states and masses were obtained from the spectral data using a home-built program[21] and MassLynx version 4.1 software (Waters). Numbers of Fe ions and Fe_2O_3 were determined by dividing mass increases by either mass of Fe (55.8 Da) or Fe_2O_3 (159.6 Da).

Received: January 22, 2009
Revised: April 7, 2009
Published online: May 19, 2009

Keywords: biomimetic synthesis · iron oxides · mass spectrometry · metal binding · protein cages

[1] T. Douglas, E. Strable, D. Willits, A. Aitouchen, M. Libera, M. Young, *Adv. Mater.* **2002**, *14*, 415 – 418.
[2] T. Douglas, M. Young, *Nature* **1998**, *393*, 152 – 155.
[3] M. Knez, A. Bittner, F. Boes, C. Wege, H. Jeske, E. Mai, K. Kern, *Nano Lett.* **2003**, *3*, 1079 – 1082.
[4] M. Uchida, M. T. Klem, M. Allen, P. Suci, M. Flenniken, E. Gillitzer, Z. Varpness, L. O. Liepold, M. Young, T. Douglas, *Adv. Mater.* **2007**, *19*, 1025 – 1042.
[5] Z. Varpness, J. W. Peters, M. Young, T. Douglas, *Nano Lett.* **2005**, *5*, 2306 – 2309.
[6] J. L. Benesch, C. V. Robinson, *Curr. Opin. Struct. Biol.* **2006**, *16*, 245 – 251.
[7] O. Esteban, R. A. Bernal, M. Donohoe, H. Videler, M. Sharon, C. V. Robinson, D. Stock, *J. Biol. Chem.* **2008**, *283*, 2595 – 2603.
[8] M. Fandrich, M. A. Tito, M. R. Leroux, A. A. Rostom, F. U. Hartl, C. M. Dobson, C. V. Robinson, *Proc. Natl. Acad. Sci. USA* **2000**, *97*, 14151 – 14155.
[9] A. J. R. Heck, R. H. H. van den Heuvel, *Mass Spectrom. Rev.* **2004**, *23*, 368 – 389.
[10] N. Kitagawa, H. Mazon, A. J. R. Heck, S. Wilkens, *J. Biol. Chem.* **2008**, *283*, 3329 – 3337.
[11] A. Ilari, S. Stefanini, E. Chiancone, D. Tsernoglou, *Nat. Struct. Biol.* **2000**, *7*, 38 – 43.
[12] E. Chiancone, P. Ceci, A. Ilari, F. Ribacchi, S. Stefanini, *BioMetals* **2004**, *17*, 197 – 202.
[13] A. Ilari, M. C. Latella, P. Ceci, F. Ribacchi, M. H. Su, L. Giangiacomo, S. Stefanini, N. D. Chasteen, E. Chiancone, *Biochemistry* **2005**, *44*, 5579 – 5587.
[14] M. Allen, D. Willits, J. Mosolf, M. Young, T. Douglas, *Adv. Mater.* **2002**, *14*, 1562 – 1565.
[15] M. Allen, D. Willits, M. Young, T. Douglas, *Inorg. Chem.* **2003**, *42*, 6300 – 6305.
[16] K. Iwahori, T. Enomoto, H. Furusho, A. Miura, K. Nishio, Y. Mishima, I. Yamashita, *Chem. Mater.* **2007**, *19*, 3105 – 3111.
[17] S. Kang, J. Lucon, Z. Varpness, L. Liepold, M. Uchida, D. Willits, M. Young, T. Douglas, *Angew. Chem.* **2008**, *120*, 7963 – 7966; *Angew. Chem. Int. Ed.* **2008**, *47*, 7845 – 7848.
[18] M. Su, S. Cavallo, S. Stefanini, E. Chiancone, N. D. Chasteen, *Biochemistry* **2005**, *44*, 5572 – 5578.
[19] R. M. Cornell, U. Schwertmann, *The Iron Oxides*, 2nd ed., Wiley-VCH, Weinheim, **2003**.
[20] S. Kang, L. M. Oltrogge, C. C. Broomell, L. O. Liepold, P. E. Prevelige, M. Young, T. Douglas, *J. Am. Chem. Soc.* **2008**, *130*, 16527 – 16529.
[21] L. Liepold, L. M. Oltrogge, P. A. Suci, M. J. Young, T. Douglas, *J. Am. Soc. Mass Spectrom.* **2009**, *20*, 435 – 442.

